Development of regional climate model for Hyogo prefecture, Japan using statistical downscaling method on CanESM2 RCP2.6, 4.5 and 8.5 scenarios

Pei Yee Ng[1], *Kok Weng* Tan[1*], and *Satoru* Oishi[2]

[1]Environmental Engineering Department, Faculty of Engineering and Green Technology, Universiti Tunku Abdul Rahman, 31900, Kampar, Perak, Malaysia.
[2]Centre for Urban Safety and Security, Kobe University, 1 Rokkodaicho, Nada Ward, Kobe, Hyogo 657-0013, Japan.

Abstract. For decades, climate models have been used to understand the present and historical climates, especially global climate models (GCMs). They are used to understand the interaction between climate system processes and forecast future climates. However, the issue of low resolution and accuracy often lead to inadequacy in capturing the variations in climate variables related to impact assessment. In order to capture the local climate changes in Hyogo Prefecture, a regional climate modelling based on Second Generation Canadian Earth System Model (CanESM2) was applied using the statistical downscaling technique. Representative Concentration Pathway (RCP) 2.6, 4.5 and 8.5 were used in generating future climate models. The reliability of three models was tested with linear regression, Pearson correlation, probability density function (PDF) and Cronbach Alpha. A moderate relationship between rainfall data and RCP4.5 was found in all chosen stations. Spatial analysis outcome showed that there is a possibility of decreased annual rainfall in the North-eastern (which city/town) and South-western (which city/town?) regions in Hyogo Prefecture.

1 Introduction

1.1 Overview

Climate change could be seen from the increase of global annual temperature and the occurring frequency of extreme weather events worldwide for the past years. According to NASA, the global averaged temperature on Earth's surface in 2020 is tied with 2016 as the hottest year ever recorded [1]. It was 1.02 ℃ higher than the baseline period of the year 1951 – 1980.

The primary factor of climate change is the greenhouse effect. Greenhouse gases (GHGs) traps solar heat and prevents it from escaping into the space, leading to global warming.

*Corresponding author: tankokweng@utar.edu.my

Examples of greenhouse gases are carbon dioxide (CO_2), methane (CH_4), and nitrous oxide (N_2O). There are two types of greenhouse gas emission sources: natural processes and anthropogenic activities. However, carbon dioxide generated from anthropogenic activities, such as deforestation and fuel combustion, is the main contributor to global warming.

The climate model could be understood as a more comprehensive weather model. It predicts over an extended period of time and forecasts how conditions in a region will change over the next several decades. Climate modelling is used in understanding the future trend of climate systems, and it allows scientists to test hypotheses and predict future climates. Also, model output helps scientists comprehend how human activity influences Earth's climate. General climate models (GCMs) are sophisticated mathematical descriptions of key components of climate systems, such as atmosphere, ocean, land surface and sea ice, and the interactions between them. However, the resolution and accuracy of GCMs, which are low, are often inadequate to record the climate variable variations, especially in impact assessments. Raw data from GCMs is difficult to be applied at local scales without downscaling due to its coarse resolution. Downscaling allows identification and analysis of extreme events, which are significant components of urban climate study [2]. Regional climate models (RCMs) are the products of downscaling, which have improved spatial and temporal resolution of the parent global models.

Besides that, currently, there is no research study on the RCMs performance in Hyogo Prefecture, Japan, based on two Representative Concentration Pathways (RCPs) scenarios, RCP4.5 and 8.5. Hence, the findings of this study will benefit society as future climate conditions are able to be predicted through the statistical downscaling method.

1.2 Objectives

This study aims to develop the local climate model (rainfall pattern 2006 – 2100) for Hyogo Prefecture based on representative concentration pathway (RCP) 2.6, 4.5 and 8.5. It is also to analyze the reliability of the downscaled model based on representative pathway (RCP) 2.6, 4.5 and 8.5 and to characterise the historical flood events in Hyogo Prefecture based on climate and human system.

1.3 Climate modelling

There are different forms of climate models, from simulating a single region of the world to those covering the major components of the entire Earth. The results of these models allow a better understanding of the effect of natural and anthropogenic activities on the Earth's climate. The projections obtained from climate modelling also assist in policy decisions on national and international scales to mitigate the impact of climate change.

GCMs represent the interaction between atmospheric, oceanic and continental phenomena with complex mathematical equations. The balance of energy between these components influences long-term climate change. In a climate model, the Earth is divided into grid cells, while specifically, in a global model, many layers are spanning across the depth and height of the sea and atmosphere [3]. A climate model with a higher resolution has more and smaller grid boxes, giving a more precise climate data output from the model for a given area.

Several examples of GCMs are CCSM4.0, CGCM4 (also known as CanESM2) and HadCM3. These models differ in terms of temporal and spatial resolution, the discretization method used, the number of vertical layers, the level of complexity in parameterizations, and the empirical choices taken. The main components of CanESM2 include an atmospheric, an oceanic, a sea-ice and two land surface models, namely Atmospheric General Circulation Model (AGCM4), Ocean GCM4, CanSim1, CTEM1 and Canadian Land Surface Scheme

(CLASS2.7). Historical simulation of CanESM2 covers 1961 – 2005, whereas the future climate projection period is 2006 – 2100.

However, GCMs are still only models despite their complexity and are limited by their capacity to accurately capture and depict each of the key processes that influence climate [3]. Thus, they are downscaled to RCMs. The regional-scale model differs from each other in terms of the nesting approach of the parent model, the parent model chose, the procedure of initialization, boundary size and type and the usage of certain noise-screening techniques [4]. GCM is able to capture the response of global circulation patterns to large-scale forcings, and RCM, for instance, is due to an increase in the concentration of GHGs. RCM could refine the information obtained spatially and temporally by considering the effects of forcings and processes in the sub-GCM grid scale.

The projection of future climatic state under different scenarios of rising atmospheric carbon dioxide (CO_2) is the most widely used application of GCMs. In IPCC AR5, Representative Concentration Pathways (RCP) 2.6, 4.5, 6.0 and 8.5 were chosen as the foundation for climate projections and forecasts. They are defined as four distinct pathways for emission of GHGs as well as air pollutants, land use and atmospheric concentrations in the 21st century [5]. RCP2.6 represents a scenario with strict mitigation; RCP4.5 and RCP6.0 are scenarios with intermediate GHG emissions, whereas RCP8.5 indicates high GHG emissions.

1.4 Statistical downscaling method

Downscaling is a process of transferring atmospheric variables changes on a large scale to a series of local weather predictands. There are two types of downscaling techniques, which are dynamical and statistical downscaling. IPCC defined dynamical downscaling as a process producing RCMs that applies over a finite domain with boundary conditions obtained from the output of GCMs [6]. It could also be defined as the process of running present GCMs at higher spatial and temporal resolution over a region of interest [7]. The main advantage of the dynamical approach is that it could resolve atmospheric characteristics of smaller scales much better than the parent GCM. Thus, dynamical models are usually more reliable in forecasting some weather extremes. However, its computational demand is as much as GCMs, in terms of applying constraints on domain size, which is feasible, the number of experiments and the simulation duration. In other words, dynamical downscaling costs much more as compared to the statistical approach.

Statistical downscaling is the empirical method of downscaling. The statistical relationships are created to link atmospheric variables on a large scale with the climate variables at the local or regional level [6]. Maraun, et al. categorized this method into three main groups, which are model output statistics (MOS), perfect prognosis (PP) and weather generation [8]. Perfect prognosis is the classic approach of statistical downscaling, comprising regression methods and weather classification. Relationships between observed large-scale atmospheric variables and observed predictands at the local scale are established. While weather generators are models that create weather time series at the local scale, having statistical properties that resemble the observed weather. The major advantage of statistical downscaling is the lower cost required due to lesser computational demand. Nonetheless, high-quality data is required to calibrate the model for a statistical approach. The assumption that the derived statistical relationships in the present will also hold under future changing scenarios might be difficult to support, resulting in uncertainties.

Feyissa, et al. downscaled a 30-year interval daily minimum temperature, maximum temperature and precipitation in Addis Ababa from Coupled Global Climate Model (CGCM3) and CanESM2 under RCP4.5 and 8.5 and Special Report Emission Scenarios (SRES) A1B and A2 using Statistical Downscaling Model (SDSM) programme [9]. Even the

precipitation changes vary seasonally; all models exhibited precipitation and temperature increase under different scenarios. RCP8.5 model performed better than SRES in predicting the precipitation amount. Moreover, Tukimat, Syukri and Malek treated an ungauged station data at Kelantan River Basin using an integrated SDSM-GIS model [10]. This study found out that the SDSM-GIS model has great potential to produce a long-term pattern of rainfall at ungauged stations. The simulated findings showed that SDSM successfully provided the long-term climatic pattern at the gauged stations with a high reliability. Generally, all RCPs projected a similar pattern of rainfall a year-round with minor intensity variations, and RCP2.6 and RCP8.5 gave the greatest and lowest long-term changes in precipitation, respectively.

2 Methodology

2.1 Study area

Hyogo Prefecture is located in Kansai Region in Japan, having Kobe as the capital. There are 29 cities *(shi)* and 12 towns *(cho)* in Hyogo prefecture. It has a total land area of 8,400.95 km^2 and a total population of 5,466,000 as of 2019. Kobe is the largest city located in Hyogo Prefecture and has Port of Kobe as one of the chief ports in Japan. Port of Kobe was established in the first year of the Meiji era, 1868, eventually became an international trading hub to Asia countries.

Population in several cities and towns in Hyogo Prefecture were obtained from Statistics Bureau of Japan, and the population growth was then calculated, shown in Table 1. It could be observed that the population in cities/towns, except Kobe City, decreased over 25 years, with the highest negative value of -16.53%. Kobe City had the highest population density of 2,742/km^2 in 2018.

Table 1. Population growth of selected cities and towns 1995 – 2015.

City/Town	1995	2000	2005	2010	2015	Growth rate, % 1995-2015	Population Density (2018)
Toyooka City	93,859	92,752	89,208	85,592	82,250	-12.37	113.9/km^2
Taka Town	1,423,792	1,493,398	1,525,393	1,544,200	1,537,272	+7.97	2,742/km^2
Kobe City	25,440	25,331	24,304	23,104	21,200	-16.53	108.6/km^2
Tatsuno City	83,431	83,207	81,561	80,518	77,419	-7.21	358.3/km^2

Japan is a country that has four seasons, which are winter, spring, summer and autumn. Its climate ranges from subarctic to subtropical in the north and south. The conditions differ between the Pacific Ocean side and the side of the Sea of Japan. Hyogo Prefecture is bounded by the Sea of Japan on the north and the Seto Inland Sea on the south. Part of Hyogo Prefecture facing the Japan Sea has an average monthly temperature that does not drop below 0 °C and experiences heavy rainfall during winter. However, the part of Hyogo prefecture that faces the Seto Inland Sea, also known as Setouchi, is warm, and rainfall amount is low throughout the year. Awaji Island, a part of Hyogo Prefecture, is the largest island found in the Seto Inland Sea.

2.2 Data collection

In this study, daily rainfall data of four stations at different regions of Hyogo Prefecture from 1980 – 2005 were obtained from Water Information System. The latitude and longitude of

the stations are shown in Table 2 and were plotted in Fig. 1. This data set was used for model calibration and validation in Statistically Downscaling Model (SDSM).

Hyogo Prefecture is located at grid cell *BOX_49X_45Y* defined by CanESM, and the 26 predictors for historical, RCP2.6, 4.5 and 8.5 were retrieved from the official website of the Government of Canada.

Fig. 1. Selected rainfall stations plotted in map.

Table 2. Rainfall stations selected.

City/Town	Region	Latitude	Longitude	Time Period
Toyooka City	Northern	35.5194 N	134.7528 E	1980 - 2019
Taka Town	Eastern	35.1375 N	134.9214 E	1980 - 2019
Kobe City	South-eastern	34.7158 N	135.2650 E	1980 – 2019
Tatsuno City	Western	34.9567 N	134.4658 E	1980 - 2019

2.3 Downscaling work

Quality control was first performed to identify missing rainfall data by the SDSM program. Missing data were treated by getting the data from the nearest station available. Then, data transformation was done with the SPSS programme. The predictands, which are the observed historical rainfall data, were screened with all 26 predictors. Predictors with significance levels lower than 0.05 and R-squared value close to 1 were chosen.

After that, observed data of 1980 – 2005 were used as predictand, and the predictor datasets obtained in predictor screening were used for model calibration. The selected period depends on the past climate conditions available for historical simulation CanESM2, which are within 1961 – 2005, whereas the projection period is determined based on the RCP scenarios, 2006 – 2100. The Scenario Generator function in SDSM was used to generate four models: the historical model, RCP2.6, 4.5 and 8.5. The generated models will then be used in model validation against the observed historical models using the Summary Statistics function in SDSM.

The simulated data will then be performed with reliability tests: Pearson correlation (r), linear regression (R2), and probability density function.

2.4 Flood analysis

Rapid and heavy rainfall causes flash floods, which increase water levels rapidly, causing rivers, channels, or streams to be overrun. River floods occur when the capacity of a river is exceeded due to persistent rain or snowmelt; whereas storm surges accompanied by tsunamis and tropical cyclones cause coastal flooding. IPCC has highlighted that if present global warming trends continue, there is a danger of increasing floods and coastal inundation resulting from rising sea levels [11]. Extreme weather and climatic events, such as floods and drought, have become more intense and frequent since the mid-20th century [12], making sustainable management of water resources even challenging than in the current stage.

Flood frequency analysis is an important procedure in hydrology, where the flood flow probabilities are determined. The concept of this analysis is that the probability of flood discharge being equalled or exceeded in any given year and the frequency of recurrence interval or return period (T) are related to the magnitude of flood discharge (Q). The inverse of the chance of exceeding a certain value of a variable in interest, for instance, river discharge and daily cumulative precipitation, is the return period [13]. Rain Intensity-Density-Frequency (IDF) curves were developed to obtain the precipitation for 2-, 5-, 10-, 25-, 50- and 100-year flood return period for each region. Based on Chow, the IDF curve could be constructed through the following equations [14]:

$$T_p = \frac{N+1}{m} \quad (1)$$

The precipitation amount had to be arranged in decreasing order of rainfall intensity, and the recurrence interval, T_p, of each observation could be obtained through equation (1), where N indicates the sample size and m represents the order number of the observation.

$$X_T = \overline{X} + K_T \sigma_X \quad (2)$$

$$\sigma_X = \sqrt{\frac{[\sum(x-\overline{x})^2]}{n-1}} \quad (3)$$

where X_T is the magnitude of the threshold level at certain return period, $\overline{X}$ represents the mean of the data, σ_X is the standard deviation of the data and K_T represents the frequency factor depending on the return period, which could be determined by the following equation:

$$K_T = \frac{y_T - \overline{y}_n}{\sigma_n} \quad (4)$$

$$y_T = -\ln\ln\left(\frac{T_r}{T_r - 1}\right) \quad (5)$$

where y_T represents the reduced variable, $\overline{y}_n$ is the reduced mean and σ_n is the reduced standard deviation. Both $\overline{y}_n$ and σ_n are function of the sample size N which could be obtained from the table.

3 Results and discussion

The validations of observation and historical climate model (1980 – 2005) are done using the SDSM programme. The comparison of average monthly rainfall and average maximum monthly rainfall at each station is illustrated in Fig. 2. There are only minor differences between observation and historical model for average monthly rainfall, where the model could be considered valid. However, for the case of average maximum monthly rainfall, major differences present between observed and simulated data, especially during year end. Underestimation issue is detected at each station. It might be due to Typhoon and extreme weather event, such as La Nina and El Nino.

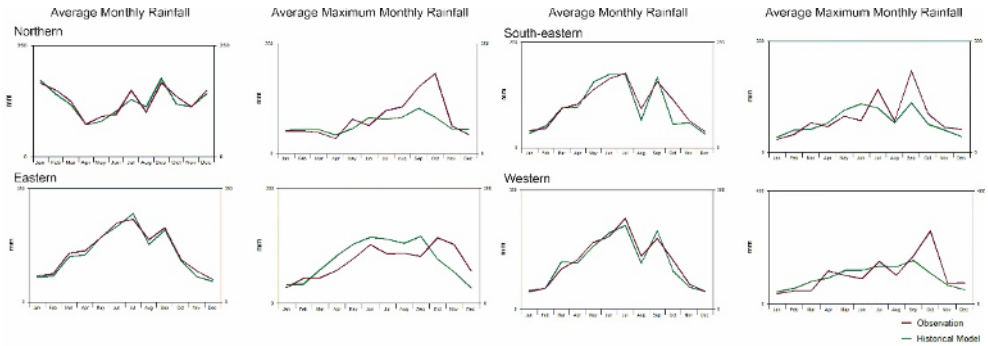

Fig. 2. Validation of average monthly rainfall and average maximum monthly rainfall of Northern, South-eastern, Eastern and Western of Hyogo Prefecture.

The outcomes from probability density function (PDF) for observation and simulated data of rainfall are shown in Fig. 3. Simulated rainfall data of each region showed similar curves and positions under observed rainfall data curve. Besides, the peak value of curves indicates the median. The medians of each PDF are similar, except RCP2.6 at the Eastern region, which is shown in Table. 3. However, PDF graphs indicated the underestimation of precipitation amount in the downscaled RCM from CanESM2.

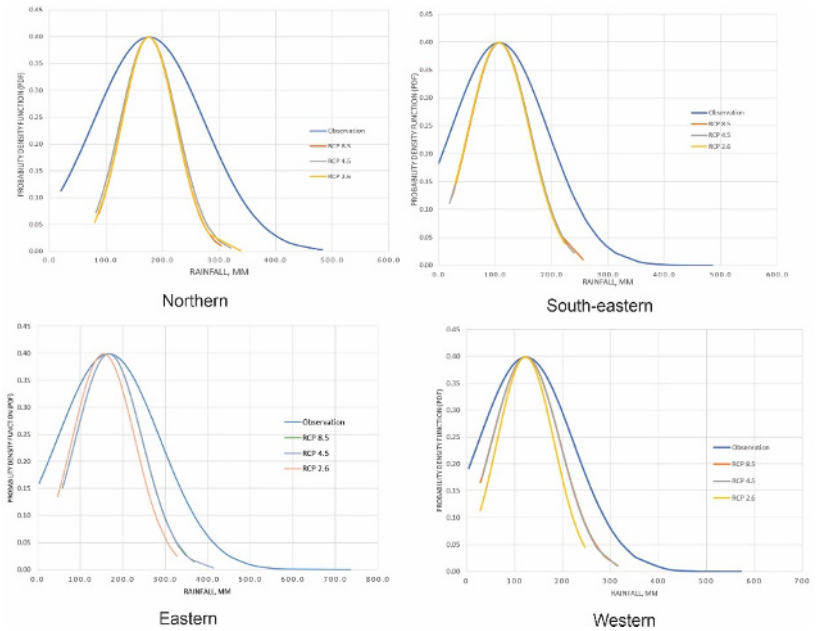

Fig. 3. PDF graphs for South-eastern, Northern, Southern and Western regions of Hyogo Prefecture.

Table 3. Peak precipitation value of each region.

Region	Northern				South-eastern				Eastern				Western			
RCP Scenarios	Obs	2.6	4.5	8.5	Obs	2.6	4.5	8.5	Obs	2.6	4.5	8.5	Obs	2.6	4.5	8.5
Peak precipitation (mm)	174.0	175.9	176.2	175.3	106.0	106.8	107.9	108.0	166.0	155.9	167.4	166.6	123.0	122.0	123.0	123.3

Values highlighted in red, shown in Table 4, indicate that the criteria assumed in experimental setup are met. All RCP scenarios for the Northern region did not pass the

reliability test, but the rest of the regions in Hyogo Prefecture show satisfactory results, which are shaded in the table. RCP4.5 is identified to meet all of the criteria. Thus, the RCP4.5 scenario is selected as a moderate relationship is found among three of the selected stations.

Table 4. Peak precipitation value of each region.

Region	Northern			South-eastern			Eastern			Western		
RCP Scenarios	**2.6**	**4.5**	**8.5**	**2.6**	**4.5**	**8.5**	**2.6**	**4.5**	**8.5**	**2.6**	**4.5**	**8.5**
Linear Regression ($r^2 \geq 0.4$)	0.18	0.19	0.21	0.28	0.40	0.37	0.30	0.40	0.35	0.41	**0.47**	0.41
Pearson Correlation Coefficients ($r_s \geq 0.6$)	0.42	0.50	0.44	0.63	**0.67**	**0.65**	0.64	**0.65**	**0.68**	**0.71**	**0.77**	**0.74**
Reliability Statistic - Cronbach Alpha ($a \geq 0.7$)	0.51	0.53	0.45	0.65	**0.73**	0.72	0.63	**0.71**	0.71	0.73	**0.79**	**0.75**

Simulated rainfall on locations away from the stations was analysed using QGIS. Fig. 4 demonstrated the spatial analysis average of the annual rainfall of Hyogo Prefecture in 20 years from 1980 – 2019 as the historical data and 2020 – 2100 as the simulated data obtained from the RCM based on RCP4.5 scenario. It could be seen that there is a possibility of reduced annual rainfall in the North-eastern and South-western region from 2020 to 2100.

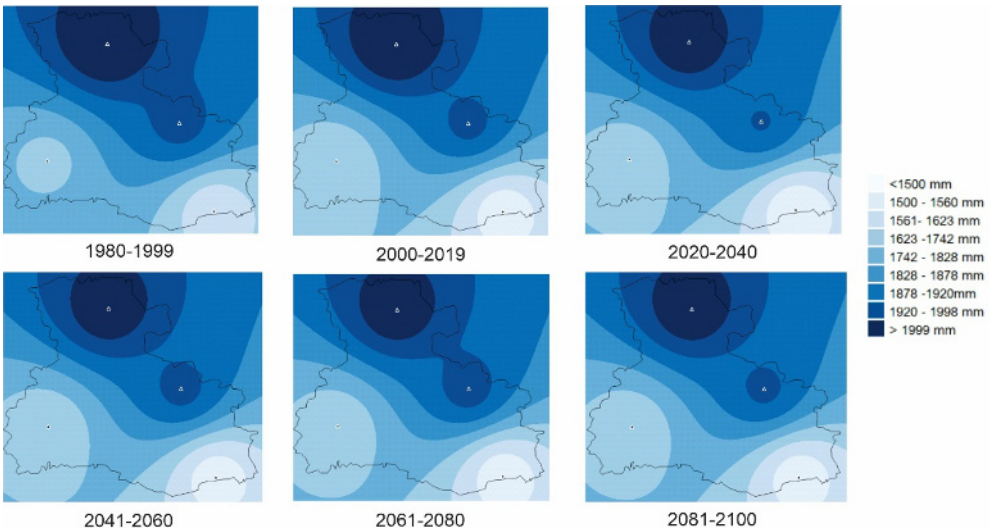

Fig. 4. The spatial analysis average of annual rainfall in 20-year period.

Rain IDF curves for each city are constructed based on observed historical data to determine the precipitation for 2-, 5-, 10-, 25-, 50- and 100-year flood return periods, shown in Fig.5. For a 1-hour storm and 100-year return period, the storm intensity at Toyooka City is 74.80 mm/hr; at Kobe City is 76.1 mm/hr; at Taka City is 88.50 mm/hr and at Tatsuno City is 70.50 mm/hr. The flood return periods are statistically different among selected stations in Hyogo Prefecture and are mainly affected by the peak value of precipitation intensity.

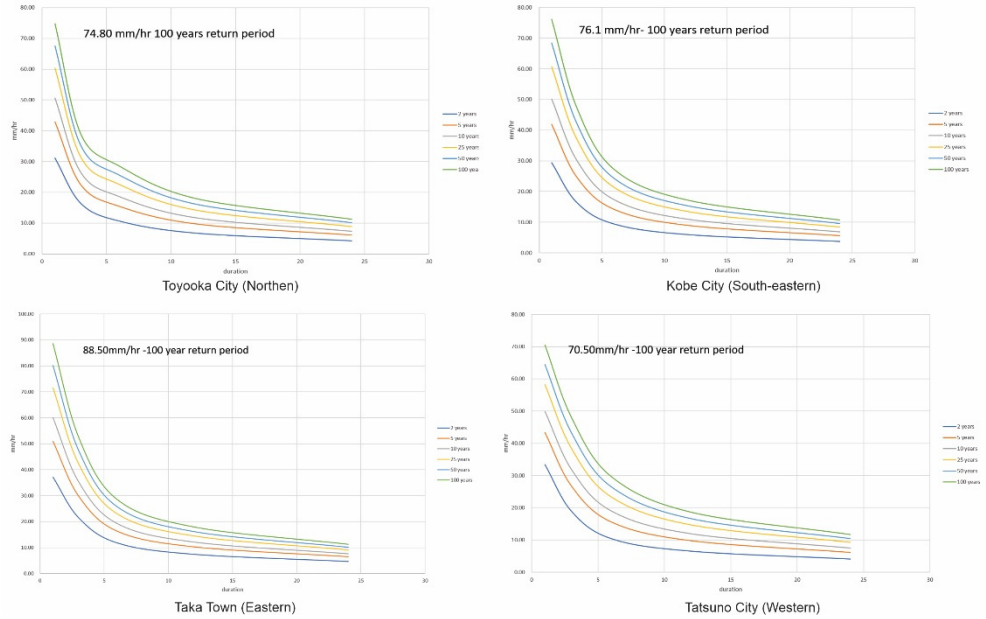

Fig. 5. Rain Intensity-Density-Frequency (IDF) curves of Toyooka City, Kobe City, Taka City and Tatsuno City.

Among four selected stations, three stations were found to experience over 300 flood events within 40 years (1980 – 2019). Cumulative distribution function curves of selected stations (Fig. 6) are plotted for observed 40-year historical precipitation data. Table 5 tabulated the analysis obtained from historical precipitation data over 40 years. The distribution of precipitation intensity in 24 hours and 1 hour for median rainfall intensity for flood events is statistically different among the monitoring stations in Hyogo Prefecture. The historical data showed that the typhoon triggered approximately 20 – 28% of the flood events. Moreover, over 75% of the flood events occurred between April and May and between August and October.

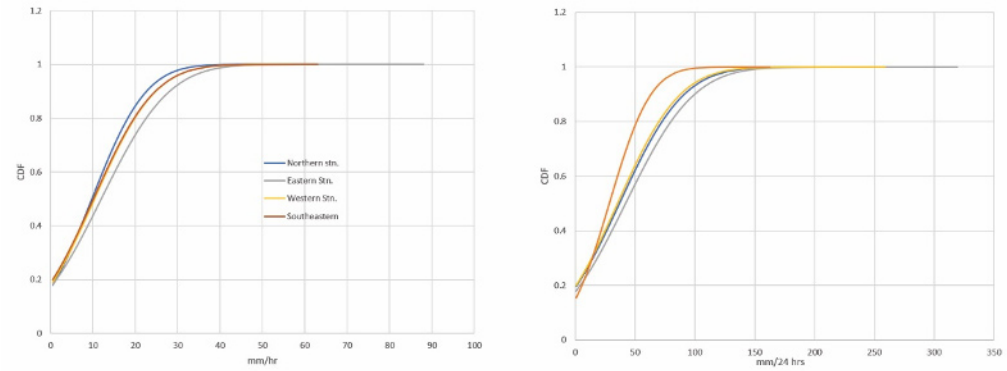

Fig. 6. Cumulative distribution function (CDF) of each station in mm/hr and mm/24hours.

Table 5. Peak precipitation value of each regions.

Region	River	Total Flood Events (1980 – 2019)	75th Percentile of Flood Events, mm/hr	75th Percentile of Flood Events, mm/24hr	Flood events by Typhoon, (%)
Northern *Toyooka City	円山川 Maruyama River	311	16.5	65.2	28
South-eastern *Kobe City	住吉川 Sumiyoshi River	241	17.8	46.8	20
Eastern *Taka Town	杉原川 Sugihara River	366	20.5	72.0	23
Western *Tatsuno City	揖保川 Ibo River	343	18.0	63.0	21

4 Conclusion

A moderate relationship is found between rainfall data and the RCP4.5 scenario in all selected stations. However, an underestimation issue is detected in the CanESM2 downscaled RCM for Hyogo Prefecture, which might be due to extreme weather events such as Typhoons during the period of season change. Based on the RCM model, there is a possibility of reduced annual rainfall in the North-eastern and South-western regions in Hyogo Prefecture in 2020 – 2100. Moreover, the rain intensity-duration-frequency (IDF) curves show that the flood return period is statically different among selected stations in Hyogo Prefecture. They are affected by the peak value of rainfall intensity. From the 40-year (1980 – 2019) observed historical precipitation data, 20 – 28% of flood events were triggered by the typhoon.

References

1. Thompson, A, SciAm, NASA says 2020 tied for hottest year on record, 14 January, United States (2021)
2. M. Dominguez, R. Romera, E. Sánchez, L. Fita, J. Fernández, P. Jiménez-Guerrero, J.P. Montávez, W.D. Cabos, G. Liguori, M.Á. Gaertner, Clim. Res., **58**, 149-164 (2013)
3. A. Lupo, W. Kininmonth, J.S. Armstrong, K. Green, *Global climate models and their limitations*, in Climate Change reconsidered II: Physical Science, NIPCC, 8 (2013)
4. F.J. Tapiador, A. Navarro, R. Moreno, J.L. Sánchez, E. García-Ortega, Armos Res, **235** 104785 (2020)
5. Core Writing Team, R.K. Pachuari, L.A. Meyer, *Climate change 2014: synthesis report*, in Fifth Assessment Report of the Intergovernmental Panel on Climate Change, IPCC (2014)
6. W.J. Merryfield, W.S. Lee, G.J. Boer, V.V. Kharin, J.F. Scinocca, G.M. Flato, R.S. Ajayamohan, J.C. Fyfe, Y. Tang, S. Polavarapu, Mon Weather Rev, **141**, 2910-2945 (2013)
7. R.A. Pielke, R.L. Wilby, Eos (Washington DC), **93**, 52-53 (2012)
8. D. Maraun, F. Wetterhall, A.M. Ireson, R.E. Chandler, E.J. Kendon, M. Widmann, S. Brienen, H.W. Rust, T. Sauter, M. Themeßl, V.K.C. Venema, Rev. Geophys., **48** (2010)
9. G. Feyissa, G. Zeleke, W. Bewket, E. Gebremariam, Climate, **6**, 58 (2018)
10. N.N.A. Tukimat, N.A. Syukri, M.A. Malek, Heliyon, **5**, e02456 (2019)
11. V. Masson-Delmotte, P. Zhai, H.-O. Pörtner, D. Roberts, J. Skea, P.R. Shukla, A. Pirani, W. Moufouma-Okia, C. Péan, R. Pidcock, S. Connors, J.B.R. Matthews, Y. Chen, X. Zhou, M.I. Gomis, E. Lonnoy, T. Maycock, M. Tignor, and T. Waterfield, *Summary for policymakers*, in Global Warming of 1.5°C, WMO, Geneva, Switzerland (2018)
12. UNESCO, The United Nations world water development report 2020: water and climate change, UN-Water, Paris (2020)

13. E. Volpi, A. Fiori, S. Grimaldi, F. Lombardo, D. Koutsoyiannis, Water Resour. Res., **51**, 8570-8585 (2015)
14. V.T. Chow, Eos (Washington DC), **32**, 231-237 (1951)